Electronic Supplementary Material (ESI) for Inorganic Chemistry Frontiers.

Electronic Supplementary Information

$Li(Na)_2FeSiO_4$/C hybrid nanotubes: **Promising anodes for lithium/**sodium **ion batteries**

Yakun Tang, Yang Gao, Lang Liu,* Yue Zhang, Jing Xie, Xingyan Zeng

Key Laboratory of Energy Materials Chemistry, Ministry of Education;

Key Laboratory of Advanced Functional Materials, Autonomous Region;

Institute of Applied Chemistry, College of Chemistry, Xinjiang University, Urumqi, 830046, Xinjiang, PR China.

Email:llyhs1973@sina.com; liulang@xju.edu.cn

Experimental Section

Synthesis of polymer nanotubes (PNTs)

To a solution of divinyl benzene (3 g) and 4-vinylbenzylchlorid (1 g) in n-heptane (100 g) was added boron trifluoride diethyl etherate complex (100 mg) at room temperature. After reacting for 10 min by ultrasonic waves, a large quantity of precipitation were produced. Then the reaction was terminated by dropping ethanol. The white fibers were filtered and washed with ethanol, leading to the polymer nanotubes (PNTs).

Synthesis of sulfonated polymer nanotubes (SPNTs)

0.2 g of PNTs were immersed in 30 mL of concentrated sulfuric acid and stirred at 50 ℃ for 12 h. The mixture was diluted by a large amount of deionized water, and the sample was collected by suction filtration and washed with water and ethanol, resulting in the sulfonated polymer nanotubes (SPNTs).

Characterization

Morphologies and structure features of the samples were studied by using field emission scanning electron microscope (FESEM Hitachi S-4800), transmission electron microscope (TEM Hitachi H-600) and high resolution transmission electron microscope (HRTEM JEOL JEM-2010F). Phase composition of the samples was characterized with X-ray diffraction (XRD, Bruker D8 advance with Cu Ka radiation). Thermogravimetric analysis (TGA) was carried out with a Netzsch STA 449C at a heating rate of 10℃ min^{-1} from 30 to 800℃ in air. Nitrogen adsorption-desorption isotherms were recorded by using an Autosorb-iQ Pressure Sorption Analyzer (Quantachrome Instruments U. S.) at 77 K. The Brunauer-Emmett-Teller (BET) method was utilized to calculate the specific surface areas. Pore size distributions were calculated by the Density Functional Theory (DFT) method. The surface

characteristics of samples were detected by an X-ray photoelectron spectroscopy (XPS, Thermo Scientific Escalab 250XI) with Al Kα radiation.

Electrochemical Characterization

2032 coin cells were used to measure electrochemical performances of the sample, with Li/Na metal as the counter and reference electrodes. A slurry consisting of 70 wt% active materials, 20 wt% carbon black and 10 wt% poly (vinylidene fluoride) binder in N-methyl-2-pyrrolidone (NMP) was casted on a Cu foil, followed by drying at 110 ℃ over night in a vacuum oven. In an argon-filled glove box, celgard 2400 membrane was used as the separator and $LiPF_6$ (1 M) in ethylene carbonate/diethyl carbonate/dimethyl carbonate (1:1:1 vol) was employed as the electrolyte [sodium ion batteries: with glass fiber as the separator and $NaClO_4$ (1 M) in ethylene carbonate/dimethyl carbonate (1:1 vol) as the electrolyte]. Cyclic voltammograms (CVs) were collected on an electrochemical workstation (CHI660D, Chenhua, China) at a scan rate of 0.1 mV s^{-1}. Galvanostatic charge-discharge tests were performed on a Land (CT2001A China) between 0.01 and 3.00 V (versus Li^+/Li, Na^+/Na). Specific capacities were calculated based on the total mass of the composite material. Full cell for LFS, a slurry consisting of 80 wt% commercial $LiFePO_4$, 10 wt% carbon black and 10 wt% poly (vinylidene fluoride) binder in N-methyl-2-pyrrolidone (NMP) was casted on a Al foil as the cathode. And the loading on the cathode was excess about three times for anode loading. Before full cell test, the anode electrode was pre-lithiation for three cycles in the half cell and disassembled in Ar glovebox. The LFS was reassembled with the commercial $LiFePO_4$ to form a full cell. The full cell was evaluated at the potential window of 0.5-3.6 V, and the specific capacity was calculated on the anode material.

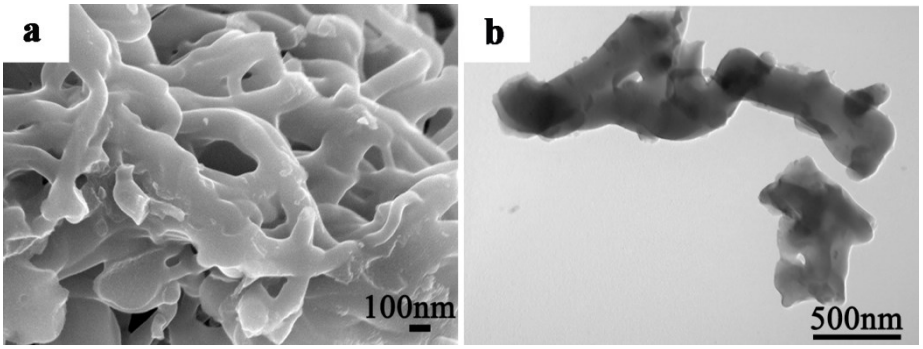

Fig. S1 SEM (a) and TEM (b) images of the carbon material obtained from SPNTs.

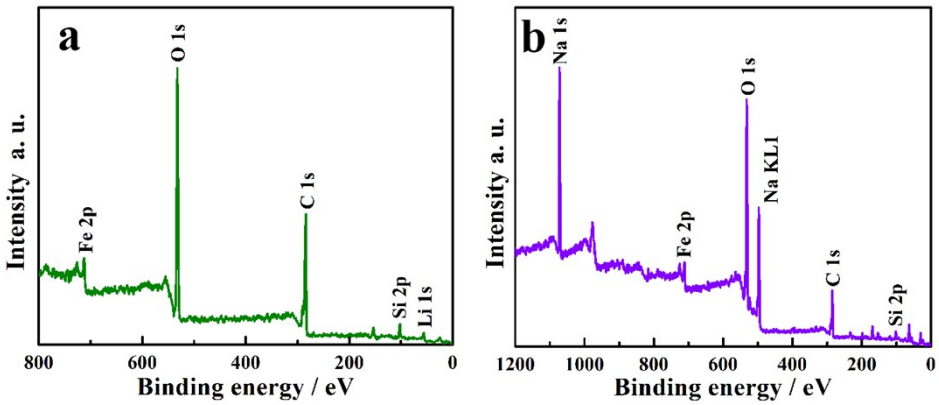

Fig. S2 XPS spectra of LFS (a) and NFS (b).

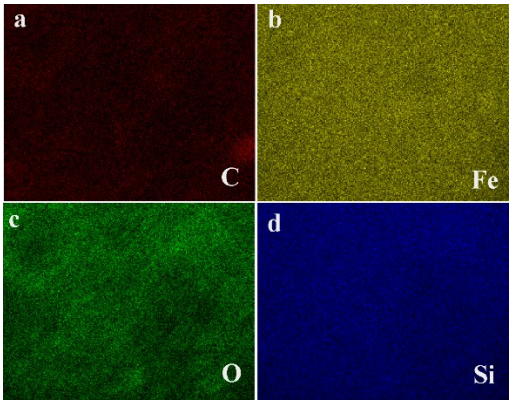

Fig. S3 EDS mappings of the LFS.

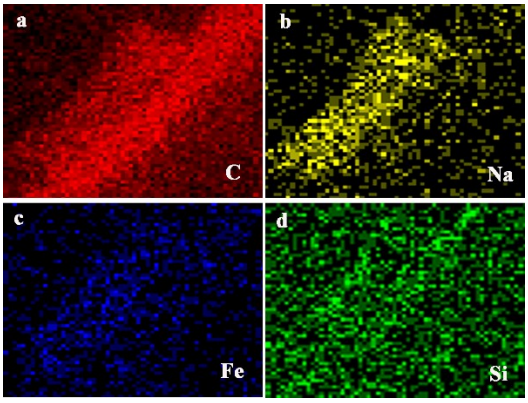

Fig. S4 EDS mappings of the NFS.

Table S1 Cycling performances and capacities of the carbon materials and $Li_4Ti_5O_{12}$-based electrodes reported in the open literature.

Typical materials	Current density (mA g^{-1})	Cycle numbers	Remaining capacity (mAh g^{-1})	Tested condition (V)	Ref.
Porous CNTs	100	150	373	0.01-3	1
N-doped porous carbon	200	---	396.7	0.005-3	2
Carbon nanoparticles network	186	---	300	0.01-3	3
Hierarchically Porous Carbon	100	700	260.1	0.01-3	4
3D hierarchical porous carbon	200	275	372	0.01-3	5
Hierarchical porous carbon microspheres	200	---	400	0.01-3	6
Carbon aerogel	200	---	400	0.01-3	7
Porous carbon spheres	200	---	400	0.01-3	8
Porous carbon sphere	37.2	100	378	0-3	9
Pollen derived carbon	186	---	350	0.01-3	10
Graphene wrapped $Li_4Ti_5O_{12}$ hollow sphere	150	---	340	0.01-3	11
CNT@$Li_4Ti_5O_{12}$ nanocable	200	200	322.5	0.01-3	12
Mg、F-$Li_4Ti_5O_{12}$	125	---	225	0-3.0	13
N-doped-C/ $Li_4Ti_5O_{12}$/Sn/TiO_2	100	---	400	0.01-3.0	14
NiO_x/$Li_4Ti_5O_{12}$	17.5	---	170	0.01-3	15
$Li_4Ti_5O_{12}$/carbon nanohybrid	17.5	---	244	0.01-3	16
V_2O_3@$Li_4Ti_5O_{12}$ particles	100	---	340	0.01-3	17
$Li_4Ti_5O_{12}$/$Ti_3C_2T_x$ nanocomposite	100	---	240	0.01-3	18
Graphene supported Li_2SiO_3/$Li_4Ti_5O_{12}$ nanocomposite	140	---	400	0.01-3	19
$Li_4Ti_{5-x}Fe_xO_{12-y}$	87.5	200	228.7	0-3	20
Carbon cloth supported $Li_4Ti_5O_{12}$@$NiCo_2O_4$ nanowire	175	---	300	0.05-3	21
$Li_4Ti_5O_{12}$-SnO_2 composites	175	200	252.3	0-3	22
LFS	200	300	444.7	0.01	

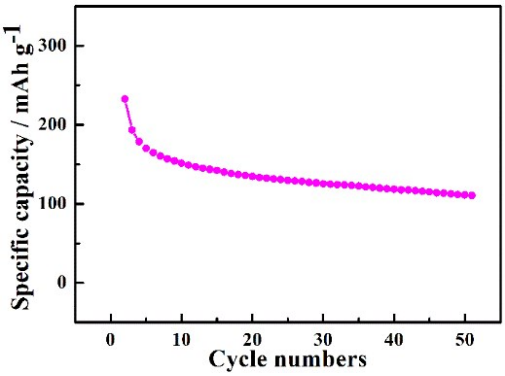

Fig. S5 Cycling stability of the full-cell with the cathodic $LiFePO_4$ and anodic LFS at 0.1 A g^{-1}.

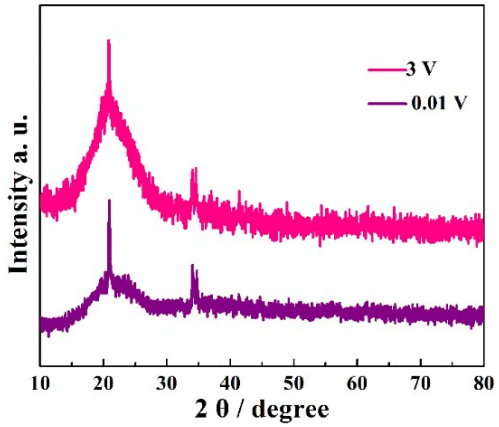

Fig. S6 Ex-situ XRD patterns of the NFS electrode at 0.01 V and 3 V during the electrochemical processes.

Table S2 Cycling performances and capacities of the sodium titanate electrodes reported in the open literature.

Typical materials	Current density (mA g^{-1})	Cycle numbers	Remaining capacity (mAh g^{-1})	Tested condition (V)	Ref.
$Na_{0.46}TiO_2$	200	---	125	0.05-2.5	23
$Na_2Ti_3O_7$@C nanofibers	177	---	135	0.01-2.5	24
Ti^{3+} doped $Na_2Ti_3O_7$	177	100	100	0.1-2.5	25
$Na_{0.23}TiO_2$ nanobelt/Ti_3C_2 MXene composites	100	---	138	0.01-2.5	26
Sodium titanate nanotube	200	200	110	0.01-2.5	27
$Na_2Ti_3O_7$@C composite	178	100	111.8	0.01-2.5	28
Twine-like $Na_2Ti_3O_7$	177	100	129.6	0.01-2.5	29
NFS	200	200	140.4	0.01-3	

References

1 M. Sahoo and S. Ramaprabhu, Effect of wrinkles on electrochemical performance of multiwalled carbon nanotubes as anode material for Li ion battery, *Electrochim. Acta*, 2015, **186**, 142-150.

2 X. J. Zhang, G. Zhu, M. Wang, J. B. Li, T. Lu and L. K. Pan, Covalent-organic frameworks derived N-doped porous carbon materials as anode for superior long-life cycling lithium and sodium ion batteries, *Carbon*, 2017, **116**, 686-694.

3 M. Kakunuri and C. S. Sharma, Candle soot derived fractal-like carbon nanoparticles network as high-rate lithium ion battery anode material, *Electrochim. Acta*, 2015, **180**, 353-359.

4 B. Capbell, R. Ionescu, Z. Favors, C. S. Ozkan and M. Ozkan, Bio-derived, binderless, hierarchically porous carbon anodes for Li-ion batteries, *Sci. Rep.*, 2015, **5**, 14575.

5 W. L. Zhang, J. Yin, Z. Q. Lin, H. B. Lin, H. Y. Lu, Y. Wang and W. M. Huang, Facile preparation of 3D hierarchical porous carbon from lignin for the anode material in lithium ion battery with high rate performance, *Electrochim. Acta*, 2015, **176**, 1136-1142.

6 F. F. Wang, R. R. Song, H. H. Song, X. H. Chen, J .S. Zhou, Z. K. Ma, M. C. Li and Q. Lei, Simple synthesis of novel hierarchical porous carbon microspheres and their application to rechargeable lithium-ion batteries, *Carbon*, 2015, **81**, 314-321.

7 X. Q. Yang, H. Huang, G. Q. Zhang, X. X. Li, D. C. Wu and R. W. Fu, Carbon aerogel with 3-D continuous skeleton and mesopore structure for lithium-ion batteries application, *Mater. Chem. Phys.*, 2015, **149**, 657-662.

8 M. Chen, C. Yu, S. H. Liu, X. M. Fan, C. T. Zhao, X. Zhang and J. S. Qiu, Micro-sized porous carbon spheres with ultra-high rate capability for lithium storage, *Nanoscale*, 2015, **7**, 1791-1795.

9 V. Etacher, C. W. Wang, M. J. O. Connell, C. K. Chan and V. G. Pol, Porous carbon sphere anodes for enhanced lithium-ion storage, *J. Mater. Chem. A*, 2015, **3**, 9861-9868.

10 J. L. Tang, V. Etacheri and V. G. Pol, From allergens to battery anodes: Nature-inspired, pollen derived carbon architectures for room- and elevated- temperature Li-ion storage, *Sci. Rep.*, 2016, **6**, 20290.
11 Z. Y. Lin, Y. M. Yang, J. M. Jin, L. W. Wei, W. Chen, Y. B. Lin and Z. G. Huang, Graphene-wrapped $Li_4Ti_5O_{12}$ hollow spheres consisting of nanosheets as novel anode material for lithium-ion batteries, *Electrochim. Acta*, 2017, **254**, 287-298.
12 Y. K Tang, L. Liu, H. Y. Zhao, D. Z. Jia and W. Liu, Porous CNT@$Li_4Ti_5O_{12}$ coaxial nanocables as ultra high power and long life anode materials for lithium ion batteries, *J. Mater. Chem. A*, 2016, **4**, 2089-2095.
13 W. Li, H. Wang, M. Z. Chen, J. J. Gao, X. Li, W. J. Ge, M. Z. Qu, A. J. Wei, L. H. Zhang and Z. F. Liu, The reaction mechanism of the Mg^{2+} and F^- co-modification and its influence on the electrochemical performance of the $Li_4Ti_5O_{12}$ anode material, *Electrochim. Acta,* 2016, **188**, 499-511.
14 S. T. Wang, Y. Yang, C. H. Jiang, Y. Hong, W. Quan, Z. T. Zhang and Z. L. Tang, Nitrogen-doped carbon coated $Li_4Ti_5O_{12}$-TiO_2/Sn nanowires and their enhanced electrochemical properties for lithium ion batteries, *J. Mater. Chem. A,* 2016, **4**, 12714-12719.
15 M. R. Jo, G. H. Lee and Y. M. Kang, Controlling solid-electrolyte-interphase layer by coating P-type semiconductor NiO_x on $Li_4Ti_5O_{12}$ for high-energy-density lithium-ion batteries, *ACS Appl. Mater. Interfaces*, 2015, **7**, 27934-27939.
16 L. Y. Zheng, X. Y. Wang, Y. G. Xia, S. L. Xia, E. Metwalli, B. Qiu, Q. Jin, S. S. Yin, S. Xie, K. Fang, S. Z. Liang, M. M. Wang, X. X. Zuo, Y. Xiao, Z. P. Liu, J. Zhu, P. M. Buschbaum and Y. J. Cheng, Scalable in situ synthesis of $Li_4Ti_5O_{12}$/carbon nanohybrid with supersmall $Li_4Ti_5O_{12}$ nanoparticles homogeneously embedded in carbon matrix, *ACS Appl. Mater. Interfaces*, 2018, **10**, 2591-2602.
17 D. N. Lei, H. Ye, C. Liu, D. C. An, J. M. Ma, W. Lv, B. H. Li, F. Y. Kang and Y. B. He, Interconnected ultrasmall V_2O_3 and $Li_4Ti_5O_{12}$ particles construct robust interfaces for long-cycling anodes of lithium-ion batteries, *ACS Appl. Mater. Interfaces*, 2019, **11**, 29993-30000.
18 C. J. Shen, Y. L. Cao, A. G. Zhou, Q. K. Hu, G. Qin, Z. P. Yang, X. Q. Liu and L. B. Wang, Novel $Li_4Ti_5O_{12}$/$Ti_3C_2T_x$ nanocomposite as a high rate anode material for lithium ion batteries, *J. Alloy. Compd.*, 2018, **735**, 530-535.
19 Q. F. Wang, S. Yang, J. Miao, M. W. Lu, T. Wen and J. F. Sun, Graphene supported Li_2SiO_3/$Li_4Ti_5O_{12}$ nanocomposites with improved electrochemical performance as anode material for lithium-ion batteries, *Appl. Surf. Sci.*, 2017, **403**, 635-644.
20 G. J. Yang and S. J. Park, Single-step solid-state synthesis and characterization of $Li_4Ti_{5-x}Fe_xO_{12-y}$ ($0 \leq x \leq 0.1$) as an anode for lithium-ion batteries, ***J. Mater. Chem. A***, 2020, **8**, 2627-2636.
21 F. H. Xu, F. L. Yu, C. Liu, P. D. Han and B. C. Weng, Hierarchical carbon cloth supported $Li_4Ti_5O_{12}$@$NiCo_2O_4$ branched nanowire arrays as novel anode for flexible lithium-ion batteries, *J. Power Sources*, 2017, **354**, 85-91.
22 M. Ding, H. Liu, J. F. Zhu, X. N. Zhao, L. Y. Pang, Y. Qi and L. Deng, Constructing of hierarchical yolk-shell structure $Li_4Ti_5O_{12}$-SnO_2 composites for high rate lithium ion batteries, *Appl. Surf. Sci.*, 2018, **448**, 389-399.
23 H. M. Li, K. L. Wang, W. Li, S. J. Cheng and K. Jiang, Molten salt electrochemical synthesis of sdium titanates as high performance anode materials for sodium ion batteries, *J. Mater. Chem. A*, 2015, **3**, 16495-16500.
24 S. Nie, L. Liu, M. Li, J. F. Liu, J. Xia, Y. Zhang and X. Y. Wang, $Na_2Ti_3O_7$/C nanofibers for high-rate and ultralong-life anodes in sodium-ion batteries, *ChemElectroChem*, 2018, **5**, 1-9.
25 T. B. Song, S. C. Ye, H. M. Liu and Y. G. Wang, Self-doping of Ti^{3+} into $Na_2Ti_3O_7$ increases both ion and electron conductivity as a high-performance anode material for sodium-ion batteries, *J. Alloy. Compd.*, 2018, **767**, 820-828.
26 J. M. Huang, R. J. Meng, L. H. Zu, Z. J. Wang, N. Feng, Z. Y. Yang, Y. Yu and J. H. Yang, Sandwich-like $Na_{0.23}TiO_2$ nanobelt/Ti_3C_2 MXene composites from a scalable in situ transformation reaction for long-life high-rate lithium/sodium-ion batteries, *Nano Energy*, 2018, **46**, 20-28.
27 X. F. Wang, Y. J. Li, Y. R. Gao, Z. X. Wang and L. Q. Chen, Additive-free sodium titanate nanotube array as advanced electrode for sodium ion batteries, *Nano Energy*, 2015, **13**, 687-692.

28 Z. C. Yan, L. Liu, H. B. Shu, X. K. Yang, H. Wang, J. L. Tian, Q. Zhou, Z. F. Huang and X. Y. Wang, A tightly integrated sodium titanate-carbon composite as an anode material for rechargeable sodium ion batteries, *J. Power Sources*, 2015, **274**, 8-14,
29 X. Yan, D. Y. Sun, J. C. Jiang, W. C. Yan and Y. C. Jin, Self-assembled twine-like $Na_2Ti_3O_7$ nanostructure as advanced anode for sodium-ion batteries, *J. Alloy. Compd.*, 2017, **697**, 208-214.